International Conference KNOWLEDGE-BASED ORGANIZATION
Vol. XXXI No 3 2025

AN ALGORITHM FOR SMALL AIRCRAFT RECOGNITION BY UNMANNED AIR VEHICLE IMAGERY

Marin MARINOV, Penyo PENEV

"Georgi Benkovski" Bulgarian Air Force Academy, Dolna Mitropolia, Bulgaria
msmarinov2016@gmail.com

Abstract: *The development of technology has made it possible to use images captured by unmanned aerial vehicles (UAVs) to recognize objects on the Earth's surface, including aircraft. The high resolution of UAV images allows the implementation of significantly simpler algorithms than those using deep learning and neural networks. The paper proposes an algorithm for small aircraft recognition based on matching with reference images of aircraft (templates). The algorithm consists of three stages. At the first stage pre-filtering of the images is carried out in order to achieve better distinction between aircraft and background. On the second stage a morphological image processing and image segmentation are applied. On the third stage a correlation processing is used to compare the detected segments potentially containing an aircraft with the templates. In all studied cases the aircraft were successfully recognized and there wasn't any false recognition.*

Keywords: remote sensing, aircraft recognition, image processing, UAV imagery

1. Introduction

The remote sensing of the Earth's surface is increasingly used in various fields of human activity. The satellite [3, 4, 7] and air vehicle [10, 17, 18] imagery is one of the key tools used for surveillance of the surface and various objects on it. The remote sensing is used for both military [2, 10, 15, 16] and civilian purposes [11, 13, 18].

One of the modern tasks of the remote sensing is aircraft detection and recognition [1, 6, 10, 14, 18]. The experience of many years of remote sensing using satellites has led to a large number of studies and to the development of different algorithms for aircraft detection and recognition [2, 4, 7].

In the last decades the technological development allows the use of aircraft for surveillance and objects detection onto ground surface [10, 17, 18].

The edge architecture, scale and shape are the most used features of aircraft [1, 3, 17]. A variety of aircraft recognition algorithms utilizing neural networks have been developed [4, 7, 10, 17]. Some of these algorithms are based on the deep learning [1, 2, 18, 19]. Using wide databases to train the neural networks, the important features of the aircraft could be extracted from images and the aircraft recognition reliability could be increased. The algorithms based on neural networks require an extensive model database of the various aircraft types and they demand significant computing power.

Most of the modern algorithms are used for large civilian and military aircraft detection on airports or in the airspace. Because of this and their complexy, the algorithms with neural networks are not suitable for the detection of small aircraft in the absence of

DOI: 10.2478/kbo-2025-0083

a reference database. Some of the techniques for object detection use handmade predefined characteristics, but because of their inherent limitations, they are not widely used.

An ever-increasing number of people could afford to purchase a small piloted aircraft nowadays. The growth of flights with small aircraft increasec the probability of accidents. They can land on unequipped grass areas, which on the one hand, allows them to land on ordinary meadows in case of emergency, but on the other hand, it makes search and rescue operations more difficult. At the same time, such aircraft could be used in illegal activities. Due to their flying at low altitudes and not always in controlled airspace, it may be necessary to search for such aircraft in unknown landing areas.

Sometimes it is important to track if an aircraft is preparing for take-off. Unmanned aerial vehicles (UAVs) are a promising tool for solving these problems.

Applications of aerial photography systems on unmanned aerial vehicles (UAV) have seen a rapid increase [14, 17] and some researchers have sought ways to simplify the algorithms for aircraft recognition [8, 9, 17]. The quality of the images from UAVs is high which allows the algorithms that utilize template matching to be used for small aircraft recognition. These algorithms rely on the unique shape of each aircraft model. Methods of image enhancement [5, 12], morphological image processing, image segmentation [5, 8] and image correlation processing [9] are used in such algorithms.

In this paper an algorithm for small aircraft recognition based on template matching is proposed. It is a combination of the modified algorithms presented in [8, 9]. The algorithm consists of three stages – pre-filtering, segmentation and template matching by correlation processing. The algorithm is applied to 66 images of two aircraft – Cessna 150 and Zlin 242L. The results show reliable recognition of both aircraft in each of the images.

2. Materials and Methods

2.1. Materials

The images used in the paper were taken by a copter UAV DJI Mini 3 Pro. It is equipped with a Global Navigation Satellite System receiver which determines the geodetic coordinates (latitude, longitude and height) of the points where images were taken and records them in the images' meta data. The camera is stabilized and has focal length $F = 6.72$ mm, aspect ratio $r = \frac{16}{9}$, an angle of view $FOV = 82.1°$, image size in height $N_r = 2268$ pixels, images size in width $N_c = 4032$ pixels. Twenty-three images of a Cessna 150 aircraft were taken at different heights from about 20 m to about 100 m at an airfield close to the city of Pleven, Bulgaria. Forty-five images of a Zlin 242L aircraft were taken at different heights from about 20 m to about 60 m at another airfield close to the city of Pleven, Bulgaria. The algorithm was implemented in MATLAB.

2.2. Image Pre-Filtering

As it was mentioned, small aircraft are often situated on grass-covered grounds. Also, the shadow that the aircraft casts on the ground is of a different shape than its. In [8], a pre-filtering algorithm is proposed that takes into account the differences in the structure of aircraft and grass images. The studies show that this algorithm doesn't work so well when the aircraft is onto an asphalt runway. A modified pre-filtering algorithm is proposed in the paper that exploits the fact that large areas of small aircraft are painted with bright colours.

On the first step the colour image is converted to greyscale image using the equation:

$$IG(i,j) = \max[I_R(i,j), I_G(i,j), I_B(i,j)], \quad (1)$$

where: $IG(i,j)$ is the brightness of the pixel in the i^{th} row and the j^{th} column of the greyscale image; $I_R(i,j), I_G(i,j), I_B(i,j)$ are the intensities of red, green and blue colours of the pixel in the original image; $\max[*]$ is the taking of maximum value.

The brightness of each pixel $IF(i,j)$ of the filtered image is formed:

$$IF(i,j) = \frac{MN_L(i,j)}{RMS_L(i,j)+IC_0}, \quad (2)$$

where: $MN_L(i,j)$ is the mean of the pixels brightness in a square area around the pixel $IG(i,j)$; $RMS_L(i,j)$ is the standard deviation of the pixels brightness in the same area; L is the number of pixels per rows and column for the area; IC_0 is a constant.

The constant IC_0 prevents the pixel value in relation (2) from becoming infinity if $RMS_L(i,j) = 0$ and it is obtained by:

$$IC_0 = MN_{RMS} + RMS_{RMS}, \quad (3)$$

where: MN_{RMS} is the mean value of the image formed by pixels $RMS_L(i,j)$; RMS_{RMS} is the standard deviation of the same image.

The size of the area is chosen in such a way that the length of the side of the square does not exceed 0.07 m:

$$L = \text{ROUND}\left(\frac{7\times10^{-2}}{\Delta_{px}}\right) \quad (4)$$

In equation (4) Δ_{px} is the pixel resolution in meters:

$$\Delta_{px} = \frac{2tg\left(\frac{FOV}{2}\right)h}{N_c\sqrt{1+\frac{1}{r^2}}} \quad (5)$$

where h is the UAV height at the moment of the picture taking.

If the number of pixels L is an even number, the area size is assumed to be L-1 pixels and if it is smaller than 3 then 3 is assumed to be the number of pixels in rows and column of the area.

2.3. Image Segmentation

Before segmentation, the filtered image **IF** undergoes some morphological operations. The first of it is a morphological gradient with square structural element $\mathbf{SE}_g$:

$$\begin{aligned}\mathbf{IMG} &= \mathbf{IF} \oplus \mathbf{SE}_g - \mathbf{IF} \ominus \mathbf{SE}_g = \\ &= \mathbf{IMD} - \mathbf{IME}\end{aligned}, \quad (6)$$

where: $\mathbf{SE}_g = \begin{bmatrix} 1 & \cdots & 1 \\ \vdots & \ddots & \vdots \\ 1 & \cdots & 1 \end{bmatrix}$ is a structural element of units with dimensions 11×11 pixels; $\mathbf{IMD} = \mathbf{IF} \oplus \mathbf{SE}_g$ is the image after morphological dilation and $\mathbf{IME} = \mathbf{IF} \ominus \mathbf{SE}_g$ is the image after morphological erosion.

The value of a pixel $IMD(i,j)$ from the image **IMD** is equal to that of the pixel with maximum brightness from a region of the filtered image **IF** that overlaps with the structural element $\mathbf{SE}_g$ whose central pixel overlaps with the pixel $IF(i,j)$:

$$IMD(i,j) = \max_{\substack{m=-5\div5 \\ n=-5\div5}}[IF(i+m,j+n)] \quad (7)$$

The value of a pixel $IME(i,j)$ from the image **IME** is equal to that of the pixel with minimum brightness from a region of the filtered image **IF** that overlaps with the structural element $\mathbf{SE}_g$ whose central pixel overlaps with the pixel $IF(i,j)$:

$$IME(i,j) = \min_{\substack{m=-5\div5 \\ n=-5\div5}}[IF(i+m,j+n)] \quad (8)$$

To smooth the contours and fill the small gaps between objects in the image **IMG** a morphological closure is used. In result the smoothed image **IMC** is obtained:

$$\mathbf{IMC} = (\mathbf{IMG} \oplus \mathbf{SE}_c) \ominus \mathbf{SE}_c, \quad (9)$$

where $\mathbf{SE}_c = \begin{bmatrix} 1 & \cdots & 1 \\ \vdots & \ddots & \vdots \\ 1 & \cdots & 1 \end{bmatrix}$ is a $L_1 \times L_1$ pixels square structural element of units.

The number L_1 of pixels in the structural element $\mathbf{SE}_c$ is calculated in such way that the length of its side does not exceed 0.21 m:

$$L_1 = \text{ROUND}\left(\frac{21\times10^{-2}}{\Delta_{px}}\right). \quad (10)$$

If the obtained number of pixels L_1 is an even number, $L_1 + 1$ is assumed to be the size of the structural element.

After morphological processing of the image **IMC** is converted to a binary image **IB**:

$$IB(i,j) = \begin{cases} 1, & IMC(i,j) > trh \\ 0, & IMC(i,j) \le trh \end{cases}, \quad (11)$$

where trh is the threshold of pixel's brightness.

The threshold is determined by the following characteristics of the image **IMC**:

$$trh = MN_{IMC} + 3RMS_{IMC}, \quad (12)$$

where: MN_{IMC} is the mean value of image **IMC**; RMS_{IMC} is the standard deviation of image **IMC**.

The last step before segmentation is filling the holes in the image. This is achieved by finding all pixels with a value of zero that are completely surrounded by pixels with a value of 1 and changing their values to 1. Standard techniques for image separation [5] are used to find the segments in the image **IBF**. The following parameters of the ellipse with normalized second central moment same as the segment are extracted:

- the coordinates of the center in pixels;
- the length of the major axis in pixels;
- the orientation of the major axis relative to the rows of the image;
- the length of the minor axis in pixels.

Due to the shape of small aircraft, the orientation of the major axis of the ellipse is close to that of the wings. Similarly, the orientation of the minor axis of the ellipse is close to that of the fuselage (longitudinal axis of aircraft). The length of the major axis of ellipse will be close to the wingspan of the aircraft, whereas the length of the minor axis will be close to the aircraft length. Considering this, the product of the axes in square meters is formulated as the first parameter for segment selection:

$$P_1 = M_{mjr}\, M_{mnr}\, \Delta_{px}^2, \quad (13)$$

where: M_{mjr} is the length of major axis in pixels; M_{mnr} is the length of minor axis in pixels.

The ratio between the two axes of the ellipse is the second parameter for segment selection:

$$P_2 = \frac{M_{mjr}}{M_{mnr}}. \quad (14)$$

The criteria for selection of segments that are likely to contain aircraft:

$$\begin{aligned} &50\ \mathrm{m}^2 \le P_1 \le 150\ \mathrm{m}^2 \\ &P_2 < 2.5 \end{aligned} \quad (15)$$

If the criteria (15) are met by a given segment, then a square region around the ellipse centre is extracted from the binary image **IBF**. The dimensions of this region are $M_k \times M_k$ and $M_k = \mathrm{ROUND}\left[1.5 M_{mjr}\,(k)\right]$ (k is the segment number). If M_k is an even number then $M_k + 1$ is taken as dimension of the k^{th} square region.

The equation (16) describes the initial estimation of the angle between the image rows and the longitudinal axis of the aircraft:

$$\gamma_k = 90° - \alpha_k, \quad (16)$$

where α_k is the angle of the major axis relative to rows of image **IBF**.

In such a way, the obtained square images $\mathbf{IBC}_k$ are prepared for correlation processing.

2.4. Image Correlation Processing

The first step of this processing is to rotate each image $\mathbf{IBC}_k$ by the angle γ_k to obtain the images $\mathbf{IR}_k$. The symmetry about the longitudinal axis of the aircraft is used to refine the rotation angle. A vector $\boldsymbol{\Delta\beta}$ of angles $\Delta\beta_i$ with values in the range $-3°$ to $3°$ and a step of $0.2°$ is created. A given image $\mathbf{IR}_k$ is rotated consequently by angles $\Delta\beta_i$ from $-3°$ to $3°$ with a step of $0.2°$. From each rotated image a matrix $\mathbf{IM}_i$ is formed with columns equal to the non-zero columns of the rotated image. The expectation of each column of the matrix is calculated:

$$y_{\Delta\beta_i}(p) = \frac{1}{\sum_{q=1}^{M_k} IM_i(q,p)} \sum_{q=1}^{M_k} q IM_i(q,p) \quad (17)$$

The symmetry of each image $\mathbf{IBC}_k$ is estimated by the standard deviation of the expectations (17):

$$\sigma(\Delta\beta_i) = \sqrt{\frac{1}{P}\sum_{p=1}^{P}\left[y_{\Delta\beta_i}(p) - \overline{y_{\Delta\beta_i}}\right]^2} \quad (18)$$

where: $\overline{y_{\Delta\beta_i}} = \frac{1}{P}\sum_{p=1}^{P} y_{\Delta\beta_i}(p)$ is the mean value of the expectations (18); P is the number of columns in the matrix $\mathbf{IM}_i$.

The residual angle $\Delta\beta$ to horizontal position of the aircraft is the angle $\Delta\beta_i$ for which the standard deviation (18) is minimal. Therefore, the refined angle of rotation is:

$$\beta_k = \gamma_k + \Delta\beta \quad (19)$$

Rotating the image $\mathbf{IBC}_k$ by the angles β_k, and resizing the rotated image to the scale of the reference image $\mathbf{I}_r$ the final image $\mathbf{I}_{ck}$ for the correlation processing is obtained. The cross correlation matrix of the two images is calculated:

$$C_k(n,l) = \sum_{m=1}^{szr}\sum_{r=1}^{szr} I_r(m,r) I_{ck}(m-n, r-l), \quad -(sz-1) \le k, l \le szr - 1 \quad (20)$$

where: szr is the number of pixels of the reference image in each row and each column; sz is the number of pixels in the rows and columns of the resized image of the k^{th} segment.

The maximum of the correlation matrix is often used as a measure of matching but this is inconsistent estimation in the case of binary images. In this paper, the following image correlation index (ICI) is used:

$$ICI_k = \frac{\max[C_k(n,l)]}{\max[C_r(n,l)]} \frac{\sigma_{C_r}}{\sigma_{C_k}}, \quad (21)$$

where: $\max[C_k(n,l)]$ is the maximum value of the cross correlation matrix; $\max[C_r(n,l)]$ is the maximum value of the autocorrelation matrix of the reference image; σ_{C_k} is the standard deviation of the cross correlation matrix; σ_{C_r} is the standard deviation of the autocorrelation matrix.

Although the aircraft in the images $\mathbf{I}_{ck}$ are horizontally aligned, they may be pointing left or right. Because of this the ICI is calculated for reference images with aircraft pointing left and right. The bigger ICI is taken for the next steps.

If the ICI for the k^{th} segment is greater than 0.5 it is assumed that there is an aircraft in this segment is made, a square placeholder of the segment is plotted in the original image and an asterisk is put in the pixel corresponding to the centre of the ellipse extracted from the segment. The correlation processing of each segment is performed with all reference images of aircraft and the model of the detected aircraft is the one for which the ICI is the largest.

As a result of algorithm application the recognition of the aircraft in image is done.

3. Results and Discussion

The reference image of each aircraft is obtained by applying the proposed algorithm to the one of the images of corresponding aircraft and selecting the square segment from the binary image that contains the aircraft. After that this square image is resized to an image with pixel resolution 0.0602 m, corresponding to a shooting height of 160 m. The resized image is recorded as a reference image for the given aircraft. An image of Cessna 150 aircraft taken at height 17.99 m is used and an image of Zlin 242L taken at height 19.53 m are used to obtain reference images.

In Figure 1 the image of a Cessna 150 aircraft taken at height 67.99 m (left) and the one of a Zlin 242L aircraft taken at height 59.83 m (right) are shown.

Figure 1: Images of Cessna 150 and Zlin 242L aircraft on two different airfields.

Figure 1 shows that in addition to the aircraft, other objects of various sizes are also observed in the images.
In Figure 2 the binary images obtained during the algorithm execution are shown. The silhouettes of the two aircraft are clearly visible and they are easily recognized by a human eye. There are artifacts on the images but their numbers are small which facilitates segmentation. The artefacts are less in the image with Zlin 242L aircraft (right). This is because the pre-filtering is more effective for grass background than for asphalt.

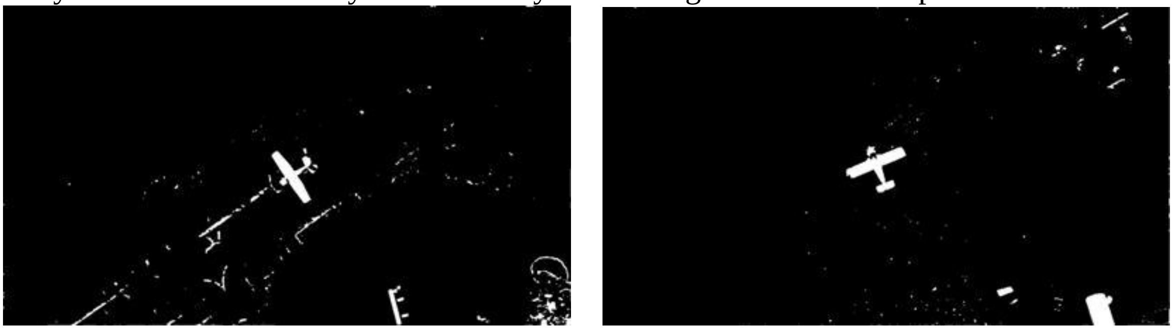

Figure 2: Binary images obtained during the algorithm execution.

The placeholders of the segments potentially containing aircraft are plotted in the original images (Figure 3). Also, asterisks are put in the centres of the ellipses corresponding to the segments. Figure 3 shows that in the left image (with Cessna 150) the placeholders contain not only aircraft but also other objects.

Figure 3: Original images with placeholder and asterisk added to them.

Figure 3 shows that the asterisks are exactly on the fuselage of the aircraft which shows that the coordinates of the ellipse centre is a good estimate of the aircraft's position in the image. In all 44 images of the Zlin aircraft only the segments with the aircraft are selected after the second stage of the proposed algorithm. From the 22 images of the Cessna aircraft in 5 of them there is more than one selected segment. The presence of segments without aircraft in them only in the images of one of the aircraft is because of the differences between the objects on the two airfields.
The values of ICI for all images are shown in Figure 4.

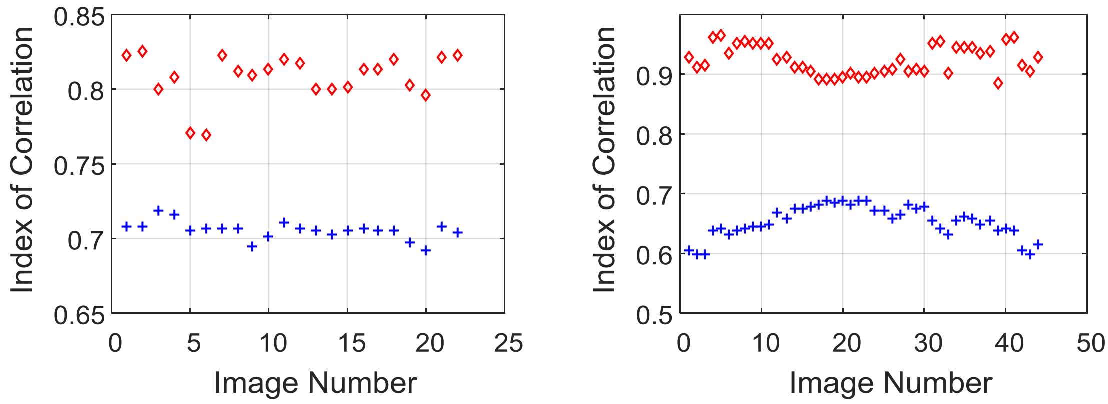

Figure 4: Indexes of correlation when different reference images are used.

In the left graphic are shown the results of 22 Cessna 150 aircraft images processing (without the image used to create a reference image) and in the right graphic the results of 44 Zlin 242L aircraft images processing (without the image used to create a reference image) are shown. The diamonds designate the ICI when segments containing aircraft are compared with the reference image of the same aircraft (for example an image of Cessna 150 is compared with a reference image of Cessna 150). With plus sign are shown the ISIs when segments containing aircraft are compared with the reference image of the other aircraft (for example an image of Cessna 150 is compared with a reference image of Zlin 242L).

The results in Figure 4 show that in all cases after correlation processing only the segments with aircraft inside them remain. There was no false recognition of aircraft or undetected aircraft. The minimum difference between the ICI with the correct reference image of a Cessna 150 aircraft and with the incorrect one is 8.96 %, whereas for a Zlin 242L aircraft this difference is 29.77%. The difference in ICIs for the two aircraft models is because of different backgrounds.

The comparison of the results in the graphics on the right in Figure 4 with the results obtained in [9] shows that the ones from modified algorithm proposed in the paper are better.

The results prove that the proposed algorithm provides a reliable and accurate recognition of Cesna 150 aircraft and Zlin 242L aircraft by processing images obtained by a small UAV.

4. Conclusions

In the paper, the small aircraft recognition problem is addressed based on a three-stage algorithm using matching with reference image. Using morphological processing and correlation of binary images the computer power demands are reduced.

The proposed algorithm was applied to 66 images and the results demonstrate a successful recognition of the aircraft in all images without any false recognition of other object as an aircraft. The algorithm shows better performance than the similar one proposed in [8,9].

Acknowledgements

This work was supported by the NSP SD program, which has received funding from the Ministry of Education and Science of the Republic of Bulgaria under the grant agreement no. Д01-74/19.05.2022

References

[1] Ashapure A, Jung J et al. A Comparative Study of RGB and Multispectral Sensor-Based Cotton Canopy Cover Modelling Using Multi-Temporal UAS Data. Remote Sensing. 2019; 11(23):2757. https://doi.org/10.3390/rs11232757.

[2] Basim Azam, Muhammad Jaleed Khan et al. Aircraft detection in satellite imagery using deep learning-based object detectors. Microprocessors and Microsystems. 2022; Volume 94: 104630. ISSN 0141-9331, https://doi.org/10.1016/j.micpro.2022.104630.

[3] Chen L., Zhou L., Liu J. Aircraft Recognition from Remote Sensing Images Based on Machine Vision. Journal of Information Processing Systems. 2020; 16(4): pp.795-808. DOI: 10.3745/JIPS.02.0136.

[4] Fu S., He Y., Du X. et al. Anchor-free object detection in remote sensing images using a variable receptive field network. EURASIP J. Adv. Signal Process. 2023; 53 (2023). https://doi.org/10.1186/s13634-023-01013-2.

[5] Gonzalez Rafael C., Richard E. Woods. Digital Image Processing. 4th Edition. New York: Pearson Education Limited; 2018.

[6] Hsieh Jun-Wei, Chen J. M. et al. Aircraft type recognition in satellite images. Vision, Image and Signal Processing, IEE Proceedings. 152(4): 2005, 307 - 315. 10.1049/ip-vis:20049020.

[7] Kang J., Tariq S. et al. A Survey of Deep Learning-Based Object Detection Methods and Datasets for Overhead Imagery. IEEE Access. 2022; vol. 10: pp. 20118-20134. doi: 10.1109/ACCESS.2022.3149052.

[8] Marinov Marin, Penev Penyo. An Algorithm for Aircraft Detection with an Empty Weight of up to 1500 Kilograms, Located on a Grass Airfields. In Annual International Sceintific Conference. Dolna Mitropolia, Bulgaria: Bulgarian Air Force Academy; October 17-18, 2024. pp. 126-140.

[9] Marinov Marin, Penev Penyo. Identification of Aircraft with an Empty Weight of up to 1500 Kilograms in UAV Imagery. In Annual International Sceintific Conference. Dolna Mitropolia, Bulgaria: Bulgarian Air Force Academy; October 17-18,. 141-150, 2024.

[10] Qiangwei Liu, Xiuqiao Xiang et al. Aircraft detection in remote sensing image based on corner clustering and deep learning. Engineering Applications of Artificial Intelligence. 2020; Volume 87:103333, ISSN 0952-1976. https://doi.org/10.1016/j.engappai.2019.103333.

[11] Petrova Teodora, Petkova-Georgieva Stoyanka, Petrov Zhivo. Improving the environmental monitoring process through the application of unmanned aerial vehicles. Journal of Environmental Protection and Ecology. 22(3): 1144-1150, 2021. ISSN 1311-5065.

[12] Petrova Teodora, Petrov Zhivo, Contrast Enhancing by Applying Histogram Analysis in Image Processing. In 22nd International Symposium INFOTEH-JAHORINA (INFOTEH). East Sarajevo, Bosnia and Herzegovina: 2023. 1-4. doi 10.1109/INFOTEH57020.2023.10094055.

[13] Petrova Teodora, Petrov Zhivo. Linear Images Coprocessing in Environmental Monitoring. In Proceedings of the 23rd International Conference on Computer Systems and Technologies. New York, USA: Association for Computing Machinery; 2022. 91–94. https://doi.org/10.1145/3546118.3546144.

[14] Sahith Jai K. Recognition of Aircraft in Remote Sensing Images Using Convolutional Neural Network. Journal of Airline Operations and Aviation Management. 2022; Vol. 1 No 1. 63-70. ISSN 2949-7698.

[15] Majumdar Sushobhan. The Role of Remote Sensing and GIS in Military Strategy to Prevent Terror Attacks. In: Subhendu Kumar P., Sanjay Kumar Si, et al. editors. Intelligent Data Analytics for Terror Threat Prediction: Architectures, Methodologies, Techniques, and Applications. Wiley; 2021. 79-94. doi:10.1002/ 9781119711629.ch4.

[16] Tan Y, Li Q. et al. Aircraft Detection in High-Resolution SAR Images Based on a Gradient Textural Saliency Map. Sensors. 2015; 15(9):23071-23094. https://doi.org/10.3390/s150923071.

[17] Tang L., Zhou S., Wang X. A Lightweight Object Detection Network for UAV Aerial Images. Frontiers in Computing and Intelligent Systems. 2024; 8(1):35-42. https://doi.org/10.54097/c5q8fv57.

[18] Wang Yanfeng, Wang Tao et al. TransEffiDet: Aircraft Detection and Classification in Aerial Images Based on EfficientDet and Transformer. Computational Intelligence and Neuroscience. 2022; vol.2022(2262549). 10 pages. https://doi.org/10.1155/2022/ 2262549.

[19] Zhang Y., Sun H. et al. Aircraft Type Recognition in Remote Sensing Images Based on Feature Learning with Conditional Generative Adversarial Networks. Remote Sensing. 2018; 10(7):1123. https://doi.org/10.3390/rs10071123.